

# Locating where Transient Signals Travel in Inhomogeneous Media<sup>1</sup>

John L. Spiesberger

*Department of Earth and Environmental Science, 240 S. 33rd St.  
U. Pennsylvania, Philadelphia, Pennsylvania 19104-6316*

e-mail: johnsr@sas.upenn.edu

31 January 2005

## ABSTRACT

Locating where transient signals travel between a source and receiver requires a final step that is needed after using a theory of diffraction such as the integral theorem of Helmholtz and Kirchhoff. Introduced here, the final step accounts for interference between adjacent apertures on a phase screen by adaptively adjusting their phase and amplitude, yielding a hierarchy of energy contributions to any desired window of signal travel time at the receiver. The method allows one to check errors in ray theory at finite wavelengths. Acoustic propagation at long distance in the oceanic waveguide (50-100 Hz, 0.05 s resolution) has significant deviations from ray theory. The boundary condition of zero pressure at the surface of the ocean appears to cause sound to travel in a nearly horizontal trajectory for a much greater distance near the surface than predicted by rays. The first Fresnel zone is an inappropriate scale to characterize where transient sounds travel near a ray path as assumed by a standard scattering theory. Instead, the Fresnel zone is too large by an order of magnitude for cases investigated here. Regions where sounds travel can have complicated structures defying a simple length scale. These results are applicable to the physics of underwater sound, optics, radio communication, radar, geophysics, and theories of wave-scattering.

PACS numbers: 42.25.Fx, 43.20.El, 43.30.Re

## I. INTRODUCTION

Methods that quantify *where* transient acoustic and electromagnetic signals propagate between a source and receiver in inhomogeneous media have numerous applications. Acoustic applications include underwater communication systems and scattering theories from fluctuations in the air, the solid Earth, Sun, and the ocean. Electromagnetic applications include the Global Positioning System, radar, and communication

---

<sup>1</sup>Portions of this work were presented at the Acoustical Society of America meeting in New York, NY in May 2004, J. Acoust. Soc. Am. 115, 2549, 2004

systems that are affected by scattering from fluctuations in the index of refraction. It is important to realize that, except for ray theory, propagation models that compute the field at a receiver from emissions at a source do not reveal *where* transient signals propagate to reach the receiver. Instead, they show what the received field is. Locating regions where transient signals travel at finite wavelength requires solving Helmholtz's equation twice, once from the source to receiver, and the other from the receiver to the source [1, 2]. The integral theorem of Helmholtz and Kirchoff uses these two solutions to estimate the received signal due to the field passing through any aperture on a phase screen between the source and receiver at finite wavelengths. This theory and that for rays have been used for more than a century. The literature on the propagation of sound in the sea appears to have a single pioneering paper discussing how a diffraction theory based on physical optics [1] compares to the theory of rays for transient signals at low frequency [3]. That paper yields paths that are ray-like, thus seeming to confirm the ray approximation. Ref. [3] uses a final step to estimate where sounds travel. Later, we will see why that final step is not quite what is needed. Without some final step following use of a theory of diffraction that utilizes two solutions to Helmholtz's equation, it may not be possible to estimate *where* transient signals propagate between a source and receiver.

This paper introduces the needed final step. It computes where transient signals propagate based on a hierarchy of energy contributions to any specified window of travel time at a receiver. The step adaptively adjusts the phase and amplitude on each phase screen to account for effects of interference of transient signals between adjacent apertures on a screen.

An interesting theory has contributed many ideas to how internal waves affect fluctuations of transient sounds in the ocean [4, 5]. The present paper checks one of the assumptions used in that theory, namely that transient signals travel within a first Fresnel zone of a ray path. This assumption was questioned by the authors of Ref. [5], but an answer appears to have not been published.

Using the needed final step introduced in this paper, we find that the Fresnel zone assumption is not valid. Actual regions where sounds travel can be complicated and defy representation by a single length scale. Although it is known that ray theory is expected to be less accurate at low frequencies, accurate quantification of error has apparently not been shown in the literature for inhomogeneous media.

From an intuitive standpoint, the Fresnel radius cannot be the correct scale to use for transient emissions. For example, consider propagation in a smooth waveguide for two signals having the same center frequency but different pulse resolutions. Assume the Fresnel radius is evaluated at the center frequency [4, 5]. Signals from a narrow pulse should remain closer to the ray than a wide pulse because the signal arrives within a narrower time window than do signals from a wide pulse. Therefore, a Fresnel zone cannot account for the behavior of signals with different bandwidths.

The unsuitability of the Fresnel radius for describing where transient signals propagate from a source to a receiver in *homogeneous* media was apparently discovered in

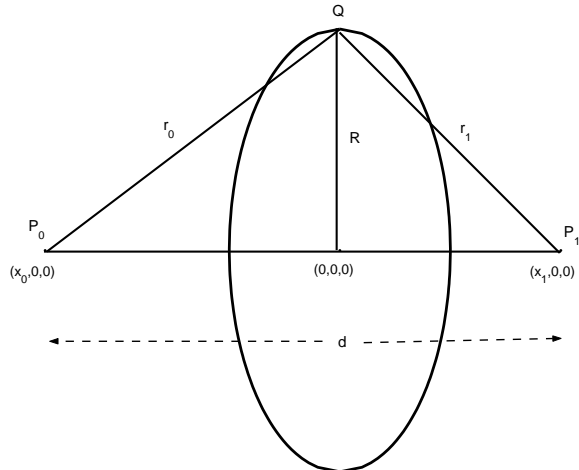


Figure 1: Geometry for calculation of acoustic field emitted at  $P_0$  and received at  $P_1$  at distance  $d$  through circular opening of radius  $R$ .

1970 in the context of geophysical exploration [6]-[9]. Later, these ideas migrated to optics where the theory was confirmed with an experiment [10]. The next question is whether this transient theory can be extrapolated to yield results for inhomogeneous media. Unfortunately but not surprisingly, the results in this paper show that propagation in inhomogeneous media is quite different than the simpler situation for homogeneous media. This paper reveals the complexities of the physics of propagation. This is an important first step toward developing theories to explain the complicated phenomena.

We start by summarizing results from the propagation of transient signals in homogeneous media. These results are applicable for some scenarios in the ocean. They also help motivate methods for quantifying where sounds travel in inhomogeneous media.

## II. HOMOGENEOUS MEDIUM: ZONE OF INFLUENCE FOR TRANSIENT EMISSIONS

Consider propagation of any transient signal originating from a point source at  $P_0 = (x_0, 0, 0)$  to a receiver  $P_1 = (x_1, 0, 0)$  through a circular opening of radius  $R$  (Fig. 1). The opening is perpendicular to the line between source and receiver, and the spatially homogeneous speed of sound is  $c$ . When the emitted signal is  $\alpha(t)$  with  $t$  denoting time, the exact solution of the acoustic wave equation is obtained using the general form of Kirchhoff's theorem for transient signals [6]-[10],

$$\mathcal{V}(t) = \frac{\alpha(t - d/c)}{d} - \left( \frac{|x_0|}{r_0} + \frac{x_1}{r_1} \right) \frac{1}{2(r_0 + r_1)} \alpha\left(t - \frac{r_0 + r_1}{c}\right), \quad (1)$$

where  $d$  is the distance between source and receiver,

$$d \equiv x_1 - x_0 . \quad (2)$$

Eq. (1) has a contribution from the signal along the straight path with geometric delay  $d/c$  plus an inverted diffracted echo traveling along the line segments  $\overline{P_0Q}$  and  $\overline{QP_1}$  with geometric-like delays of  $r_0/c$  and  $r_1/c$  respectively (Fig. 1). Interference occurs between the geometric and diffracted echo as long as they are separated by less than the temporal resolution of the signal,  $T$ . When the radius of the circle exceeds  $R = R_I$ , the two contributions are separated in time where the first contribution,  $\alpha(t-d/c)/d$ , is that obtained from propagation in a homogeneous medium without screens or boundaries. Thus, the region of space traversed by propagation in a homogeneous medium without screens is,

$$R = R_I(x) = \frac{1}{2} \frac{[cT(2|x| + cT)(2|d - x| + cT)(2d + cT)]^{1/2}}{d + cT} . \quad (3)$$

For  $cT \ll x$  and  $cT \ll d - x$ ,

$$R_I(x) \cong \sqrt{\frac{2cTx(d - x)}{d}} . \quad (4)$$

where  $x \equiv |x_1|$ . The diffracted echo vanishes as the radius of the circle goes to infinity, but in any case has no effect on the free-space solution for  $R \geq R_I$ . The diffracted component that reflects from the edge of the opening is consistent with the ideas from the geometrical theory of diffraction [11].

Eq. (4) has the same form as the Fresnel radius,

$$R_f = \sqrt{\frac{\lambda x(d - x)}{d}} . \quad (5)$$

when the pulse resolution,  $T$ , is replaced by half the period of the single frequency,  $\lambda/2c$  where the monochromatic wavelength is  $\lambda$ . Note,  $R_I/R_f$  is  $\sqrt{2Q}$  where  $Q$  is the quality of the signal so there is not much difference unless  $2Q$  is large. Significantly, Eq. (3) only depends on the temporal resolution. It does not depend on the center frequency as does the Fresnel radius.  $R_I$  is called the ‘‘zone of influence’’ [8].

This paper considers where signals travel from a source that contribute energy to a received travel time within one pulse resolution. This gives rise to the concept of the zone of influence which is the relevant physical scale of interest in this paper. This is not the same as the generalization of the Fresnel radius for transient signals [10]. The generalized Fresnel radius has a different value than the radius for the zone of influence for homogeneous media. Additionally, the generalized Fresnel radius approaches the Fresnel radius as the bandwidth goes to zero. However,  $R_I$  properly goes to infinity as the bandwidth goes to zero because the pulse resolution goes to infinity thus admitting sound from an infinite distance for an infinitely long pulse.

### III. DIFFRACTED REGIONS IN INHOMOGENEOUS MEDIA

The contribution to the time series at time  $t$  at the receiver from the wave field passing through a transparent opening between depths  $z_r$  and  $z_s$  in an otherwise opaque vertical screen at horizontal coordinate  $x_{sc}$  is,

$$\mathcal{G}_j(t, x_{sc}, z_r, z_s) = B_j \mathcal{F} \left\{ \int_{z_r}^{z_s} \int_{-\infty}^{\infty} I_j(x_{sc}, z, \omega) \exp(-i\omega t) d\omega dz \right\}; \quad j = 1, 2 \quad (6)$$

where  $B_j$  is a normalization constant and  $\omega$  is the radian frequency. The function  $\mathcal{F}$  removes the carrier frequency as in Eq. (47) of Ref. [12] via complex demodulation of analytic signals. The subscript  $j$  denotes that diffraction is estimated from the integral theorem of Helmholtz-Kirchhoff [1, 2] in which case,

$$I_1(x_{sc}, z, \omega) = W_1(x_{sc}, z, \omega) \frac{\partial W_0(x_{sc}, z, \omega)}{\partial x} - W_0(x_{sc}, z, \omega) \frac{\partial W_1(x_{sc}, z, \omega)}{\partial x} \quad (7)$$

or from physical optics<sup>1</sup> in which case,

$$I_2(x_{sc}, z, \omega) = W_0(x_{sc}, z, \omega) W_1(x_{sc}, z, \omega), \quad (8)$$

(Eqs. 18,23 of Ref. [3]). The solutions of the Helmholtz equation on the screen due to emissions located at the source and receiver are  $W_0(x_{sc}, z, \omega)$  and  $W_1(x_{sc}, z, \omega)$  respectively [1, 2]. In this paper, the inclination factor [1] for physical optics is set to unity because the direction of signal propagation is almost perpendicular to the phase screens.

Let the ‘‘region of diffraction’’ denote locations where sounds travel. This region was estimated for oceanic propagation [3] by contouring a normalized function of Eq. (6),

$$\tilde{\mathcal{G}}_j(t, x_{sc}, z) \equiv \frac{\mathcal{G}_j(t, x_{sc}, z, 0)}{\mathcal{G}_j(t, x_{sc}, -D, 0)}; \quad j = 1, 2, \quad (9)$$

where  $D$  is the depth of the bottom of the phase screen at horizontal coordinate  $x = x_{sc}$ . The bottom of the phase screen is chosen such that no significant energy propagates to the receiver below  $D$ . The top of the phase screen is set at the pressure release surface of the ocean,  $z = 0$ . The function,  $\tilde{\mathcal{G}}_j(t, x_{sc}, z)$ , goes from zero at  $z = 0$  to unity at  $z = D$  but not necessarily in a monotonic fashion.

Three innovations are introduced that yield accurate estimates of the region of diffraction based on a hierarchy of energy contributions at the receiver. Firstly, we consider the diffracted region responsible for the energy arriving between  $t \pm T/2$  at the receiver instead of the region responsible for the energy at time  $t$  as before [3]. Secondly, a method is provided for drawing boundaries of diffracted regions based on a calibration with results from homogeneous media instead of apparently choosing arbitrary boundaries [3]. Thirdly, an adaptive method is introduced for computing the contribution of each aperture on a phase screen to the energy arriving within  $t \pm T/2$

at the receiver. This method properly accounts for significant effects of interference between apertures on a screen. Ref. [3] apparently suppressed ripples of  $\tilde{\mathcal{G}}_j(t, x_{sc}, z)$  in Eq. (9) because they were believed to be caused by the interference of separate paths (p. 2667 of [3]). We show that ripples can be due to other phenomenon, such as self-interference within a resolved path, and should be not suppressed nor are they undesirable. Instead, the ripples are critical to measure to obtain a proper accounting of the energy passing through any aperture on the way to the receiver. A demonstration is given first for propagation in a homogeneous medium.

Assume a source and receiver are placed at 2 km depth in the sea and separated by 9.129 km over a flat bottom at 5.6 km. To minimize sidelobes in the time domain, a Hann taper is applied in the frequency domain to the emitted signal between  $100 \pm 40$  Hz. The taper is zero at 60 and 140 Hz, yielding an effective bandwidth of 40 Hz and a time resolution of  $1/40 = 0.025$  s. The speed of sound is 1.5 km/s. The theoretical time for the horizontal path to reach the receiver is  $9.129/1.5 = 6.086$  s. The next path at 6.645 s corresponds to energy that reflects once from the surface. The path that reflects once from the bottom has a travel time of 7.751 s. All three paths are temporally resolved with the pulse resolution of 0.025 s.

The  $c_0$  insensitive parabolic approximation [12] yields estimates of  $W_i(x_{sc}, z, \omega)$  ( $i=0,1$ ) and its derivative for each aperture through Eq. (6) for both  $j = 1, 2$ . This parabolic approximation yields accurate travel times, is efficient due to its split-step algorithm, and obeys reciprocity. It is important that reciprocity is obeyed because a proof for reciprocity is provided by the integral theorem of Helmholtz and Kirchhoff. Computational grids in depth and range are made sufficiently small to achieve convergence of the solution.

Consider the phase screen half-way between the source and receiver (Fig. 2A). Cumulative vertical contributions from this screen within times  $t \pm T/2$  can be examined with,

$$\tilde{\rho}_j(z) \equiv \max_{t \in (t \pm T/2)} \{ \tilde{\mathcal{G}}_j(t, x_{sc}, z, 0) \} , \quad (10)$$

which is zero at the surface and unity at the bottom of the phase screen ( $z=-D$ ). This function increases monotonically until just after 2 km at which point interference is observed (Fig. 2A). The apertures on this screen are about 0.02 km wide, so there are about 300 of these between the surface and the bottom of the screen at 6 km. The radius of the zone of influence at this location is about 0.4 km (Eq. 4), so contributions from the screen should die out at depths of  $2 \pm 0.4$  km, and they do. If adjacent apertures did not interfere, the contribution at the receiver from aperture  $p$  would be  $\tilde{\rho}_j(z_p) - \tilde{\rho}_j(z_{p-1})$  (Fig. 2B).

Effects of interference for the homogeneous case are illustrated after describing the following new algorithm which requires no intervention from an operator to determine how to deal with interference. It provides high-resolution images of an objective function through a finite difference of cumulative contributions of apertures with depth *after* properly dealing with decreasing values of the function with depth, if any. In this

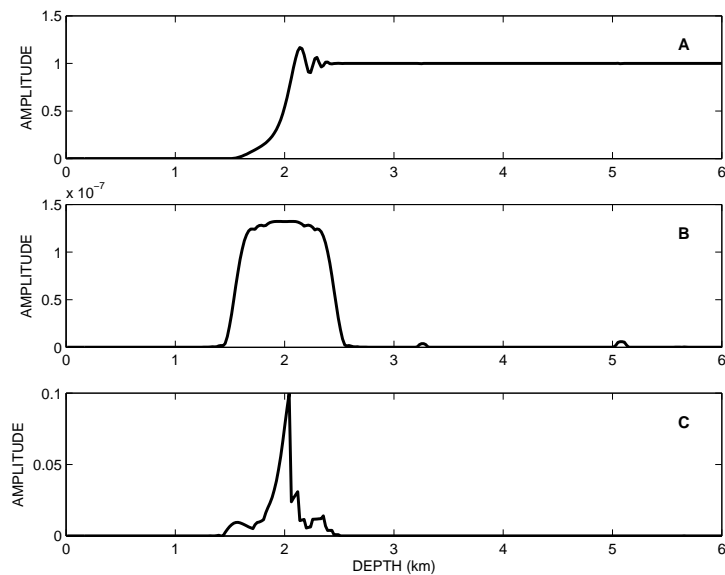


Figure 2: Example of how interference on a phase screen affects calculations of where sounds travel between a source and receiver in homogeneous media. The distance between source and receiver is 9.123 km and both are at a depth of 2 km. The speed of propagation is 1.5 km/s. The vertical phase screen is at 9.123/2 km range. Calculations are for the first (direct) path using a time window with the pulse resolution of 0.025 s. (A) The maximum value of the received time series within the time window as a function of depth on the phase screen starting from the surface and working downward (Eq. 10). (B) Contributions to the energy of the received pulse as a function of depth on the screen if adjacent apertures did not interfere destructively at the receiver. (C). Contributions to energy when interference is accounted for via Eq. (12).

sense, the output of the algorithm is formed in the same way as a probability density function which is obtained by differentiating a cumulative distribution function.

Starting from the surface, Eq. (6) is computed to the bottom of the first and second aperture,  $z_1^+$  and  $z_2^+$ , respectively. The plus sign denotes downward integration from the surface. The contribution at the receiver is computed for both integrals for the nonlinear objective function of the time series,

$$\rho_j(0, z^+) \equiv \max_{t \in (t \pm T/2)} \{ \mathcal{G}_j(t, x_{sc}, z, 0) \} ; z = z_1^+, z_2^+ . \quad (11)$$

If  $\rho_j(0, z_2^+) \geq \rho_j(0, z_1^+)$ , then we proceed on. Otherwise, destructive interference is winning so as to decrease the net contribution to the objective function. The remedy is to consider the contribution to the objective function from both apertures together instead of separately by replacing their Fourier coefficients,  $\int_0^{z_1^+} I_j(x_{sc}, z, \omega) dz$  and  $\int_{z_2^-}^{z_2^+} I_j(x_{sc}, z, \omega) dz$ , with their average, namely,  $(\int_0^{z_1^+} I_j(x_{sc}, z, \omega) dz + \int_{z_2^-}^{z_2^+} I_j(x_{sc}, z, \omega) dz) / 2$ . Replacing the separate values by their average does not change the sum of the contributions from apertures 1 and 2 to either the time series at the receiver or to the objective function because the integral from 0 to  $z_2^+$  is unaltered.

The next step compares  $\rho_j(0, z_3^+)$  with the newest value of  $\rho_j(0, z_2^+)$ . If  $\rho_j(0, z_3^+) \geq \rho_j(0, z_2^+)$ , then we continue on-wards. Otherwise, destructive interference is reducing the contribution to the objective function at the receiver. The remedy is similar to before. Fourier coefficients from apertures two and three are replaced by their mean, and this mean is retained unless  $\rho_j(0, z_2^+) \leq \rho_j(0, z_1^+)$  where the last inequality is based on the newly replaced mean value of the Fourier coefficients (it is necessary to go back and check this because the Fourier coefficients for aperture two just got modified and one wants to make sure that the jump from aperture 1 to apertures 1 plus 2 still gives a non-decreasing contribution at the receiver). If this last condition is true (destructive interference is winning), then it is necessary to replace the Fourier coefficients of apertures 1, 2, and 3 by the mean of their newest values, which guarantees that contributions from each cumulative aperture going from 1 through 3 yields non-decreasing values of  $\rho_j(0, z^+)$ . This procedure continues until the bottom of the phase screen is reached. The contribution to the objective function at the receiver from each aperture  $q$  is provided by the finite difference,

$$\delta\rho_j(q)^+ \equiv \rho_j(0, z_q^+) - \rho_j(0, z_{q-1}^+) ; q = 2, 3, 4, \dots P , \quad (12)$$

and for  $q = 1$ ,  $\delta\rho_j(1)^+ \equiv \rho_j(0, z_1^+)$ . These values are guaranteed to be non-negative as desired. Fig. (2C) shows that the greatest contributions to the peak of the time series occur over a narrower depth range than obtained if one assumes that the apertures do not interfere (Fig. 2B). Panel C displays a slight bias in the center location of the peak which should ideally occur at a depth of 2 km. The bias is suppressed by conducting the procedure leading to Eq. (12) from the bottom of the phase screen to the surface, yielding values of  $\delta\rho_j(q)^-$ , and then averaging from both directions,

$$\delta\rho_j(q) = [\delta\rho_j(q)^+ + \delta\rho_j(q)^-] / 2 . \quad (13)$$

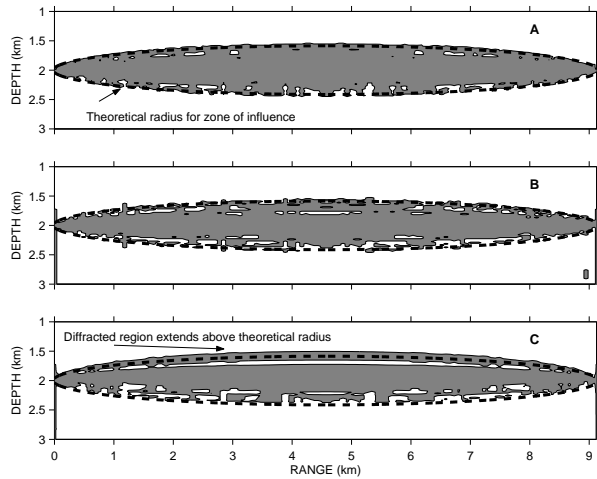


Figure 3: Three methods for estimating a region of diffraction in a homogeneous medium using the integral theorem of Helmholtz and Kirchhoff. Source and receiver are at a depth of 2 km. (A). The relative dB method uses the top  $X_{dB} = -23$  dB contributing apertures on each phase screen based on the values in Eq. (13). (B). Same except the contributions from each aperture are sorted in non-increasing order and used until a fraction of  $f = 0.90$  of maximum amplitude of the time series is reached (fractional amplitude method). (C) Same as (A) except the spatial bias is not suppressed because the phase screen is only smoothed from the top down (Eq. 12). Note the region of diffraction extends slightly above the theoretical radius of the zone of influence (Eq. 3) for a homogeneous medium.

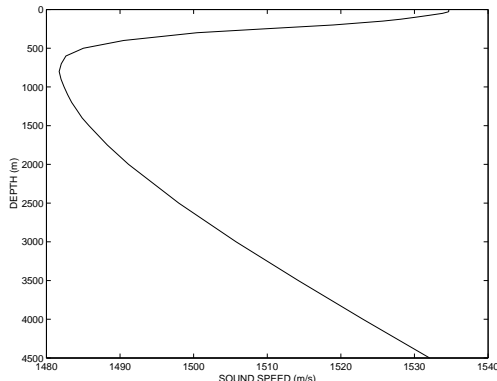


Figure 4: The speed of sound as a function of depth near Kaneohe Bay, Oahu (21.512 °N and 202.228 °E) according to climatology [13] for Spring and using Del Grosso’s algorithm for the speed of sound in seawater [14]. Straight lines are drawn between data points here, but the calculations use a quadratic spline [17] that has no discontinuities in gradient with depth.

Two methods are described for estimating a diffracted region from Eq. (13). The “relative dB” method uses all apertures within  $X_{dB}$  of the value of the maximum contributing aperture on a phase screen. The “fractional amplitude” method sorts aperture contributions in non-increasing order, then selects the minimum number of these sorted contributions from largest to smallest until reaching a specified fraction,  $f$ , of the maximum amplitude of the peak of the time series at the receiver. Values for  $X_{dB} = -23$  dB and  $f = 0.9$  fit the theoretical value of the zone of influence in a homogeneous medium fairly well (Fig. 3). The size of the diffracted region is not sensitive to the values chosen for  $X$  and  $f$ . The spatial bias of the diffracted region is suppressed when values of  $\delta\rho_j(q)$  are used (Fig. 3A) instead of  $\delta\rho_j(q)^+$  (Fig. 3C). The diffracted region has holes that indicate non-monotonic variations in sonic level within the zone of influence (Fig. 2C), indicating interference between sound traveling along the direct path and sound traveling along a diffracted path near the periphery and back to the receiver. Therefore, effects of diffracted echoes are evident even in the absence of an edge on a circular opening (**Sec. II**).

#### IV. REGIONS OF DIFFRACTION FOR WAVEGUIDE PROPAGATION IN THE OCEAN

Consider climatological conditions for Spring [13] for the North Pacific near Kaneohe Bay, Oahu (21.512 °N and 202.228 °E). Sound speeds, which only vary with depth, are estimated from temperature, salinity, and depth using Del Grosso’s algorithm [14] (Fig. 4). The acoustic models described below propagate the acoustic field in Cartesian coordinates after applying the Earth flattening transformation to the field in Fig. (4).

Four cases are considered. The purpose of the first three is to see if the region of diffraction becomes more ray-like with increasing frequency. The emitted signal has a bandwidth of 20 Hz and the center frequency is set at 50, 100, and 200 Hz. The equivalent pulse resolution is given by the inverse bandwidth, 0.05 s.

The purpose of the fourth case is to see how the region of diffraction decreases with decreasing pulse width. The case repeats the 100 Hz center frequency emission, but the bandwidth is increased to 40 Hz, yielding a narrower resolution of 0.025 s.

Assume the source and receiver are separated by 523.845 km and placed at 800 m depth, corresponding to the minimum speed (Fig. 4). The bottom is at 4500 m. As before, the signal is tapered with a Hann filter in the frequency domain to suppress sidelobes in the time domain. Attenuation of sound by seawater is accounted for as a function of frequency.

The sound-speed insensitive parabolic approximation [12] incorporates a geoacoustic bottom that is specified as follows. The sediment thickness is 200 m. The ratio of sound speed and density at the top of the sediment layer to that at the bottom of the water column are 1.02 and 1.7 respectively. The attenuation in the sediment is  $\alpha(f) = 0.02f$  (dB/m) where  $f$  is acoustic frequency in kHz. The speed increases with depth at a rate of  $1 \text{ s}^{-1}$  in the sediment. The ratio of sound speed and density at the top of the basement to that at the bottom of the sediment are 2 and 2.5 respectively. The attenuation in the basement is  $\alpha(f) = 0.5f^{0.1}$  (dB/m).

The software for the sound-speed insensitive approximation has been used before to identify broadband signals over basin-scales [16]. It yields travel times that agree with exact solutions from normal modes within a few milliseconds over basin-scales for speeds that vary with depth only [12].

Regions of diffraction are compared with rays. The ray program, zray, and its eigenray finder have been described and successfully used to study acoustic propagation for many experiments [16, 17]. Its results agree with analytical solutions. Sound speeds used by the ray program are the same as those used by the parabolic approximation on its computational grid. Between grid points, the speed is obtained using a quadratic spline. The spline goes through each grid point, and has no gradient discontinuities [17].

Attention is focused on two peaks that are temporally resolved at 0.05 s resolution (Fig. 5) (Table I). Each peak is due to a single resolved ray. These peaks appear in all four cases except at 50 Hz where peak 1 is not present because of the interaction of low frequency sound with the sub-bottom (Fig. 5B).

| PEAK | TRAVEL TIME (s) | # Turns | ANGLE (DEG.) | SHALLOWEST DEPTH (M) |
|------|-----------------|---------|--------------|----------------------|
| 1    | 352.022         | 19      | 14.093       | 130                  |
| 2    | 352.577         | 19      | -12.577      | 214                  |

**Table I.** Ray parameters for the two peaks shown in Fig. (5). The angle is that with respect to the horizontal at the source depth of 800 m. The shallowest ray depth is indicated.

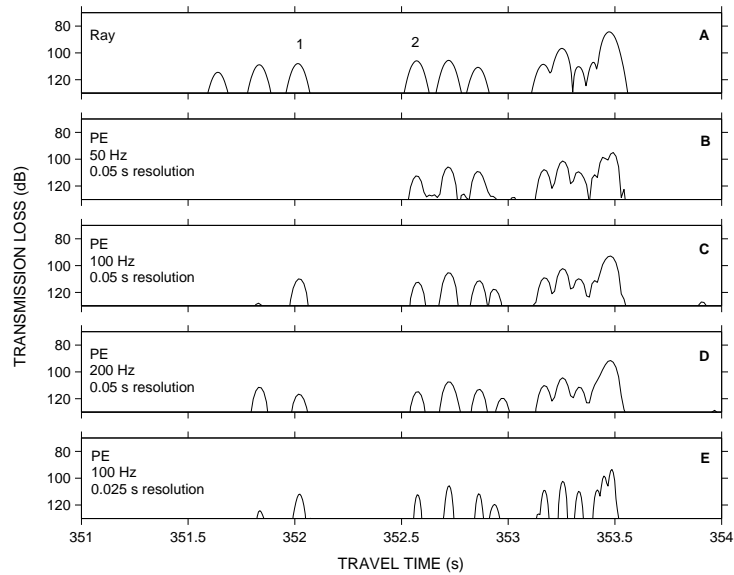


Figure 5: Impulse responses from five models between a source and receiver separated by 523.845 km and depths of 800 m with peaks 1 and 2 indicated. The top panel comes from tracing rays through the profile in Fig. (4). The next four panels are obtained using the sound-speed insensitive parabolic approximation [12] (PE) for the same field of speed as the rays. The center frequencies for the PE runs are 50, 100, and 200 Hz (panels B, C, D) with a pulse resolution of 0.05 s. Panel E has a center frequency of 100 Hz and a pulse resolution of 0.025 s.

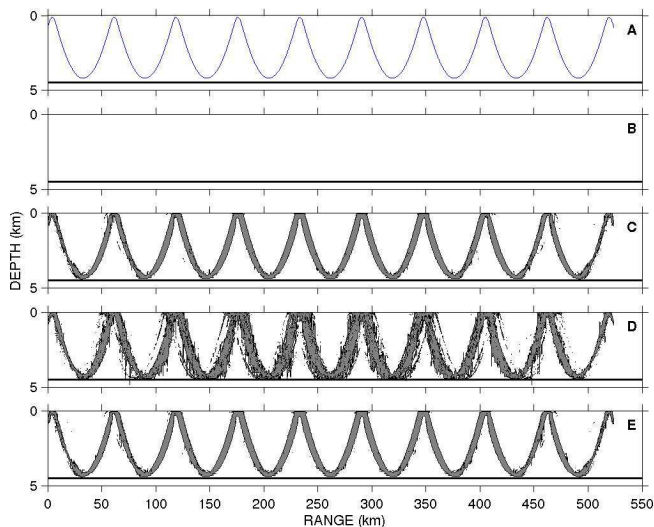


Figure 6: Paths for peak 1 for the same cases in Fig. (5) respectively. The top panel is the ray, and the others from the integral theorem of Helmholtz and Kirchhoff (Eq. 6,  $j = 1$ ) using the relative dB method and Eq. (13) to estimate the energy contributions from each 0.0195 wide vertical aperture on each phase screen. The depth of the bottom at 4.5 km is indicated. Panels B-D are for center frequencies of 50, 100, 200 Hz respectively with pulse resolution of 0.05 s. Panel E is for a center frequency of 100 Hz and a pulse resolution of 0.025 s. Peak 1 does not occur at 50 Hz due to interaction of sound with the bottom (Fig. 5).

The integral theorem of Helmholtz and Kirchhoff is used to compute the results in this section via Eq. (6). However, results based on physical optics look almost identical (not shown). Using the relative dB method that accounts for interference on phase screens (Eq. 13) diffracted regions for the peaks look somewhat like their ray paths with significant discrepancies in many cases (Figs. 6-7). The vertical stripes occurring at some ranges indicate that a wide range of depths contribute to the relative dB method at the -23 dB threshold on some phase screens. All diffracted regions show that sound extends over a flatter and more extended horizontal region near the surface than their ray counterparts (e.g. 40 km instead of  $O(1)$  km for peak 2 in Fig. 7). Peak 1 (Fig. 6C,D) looks less ray like at 200 Hz than 100 Hz (Fig. 6). Peak 2's upper turning regions look like they have antlers that extend the exposure to the surface region, particularly at a center frequency of 50 Hz (Fig. 7B). The bottoms of the diffracted regions appear to have attachments of broadly shaped "V's" that are more pronounced at mid range than near the source or receiver. These "V's" are suppressed when the pulse resolution is changed from 0.05 to 0.025 s (Fig. 7E).

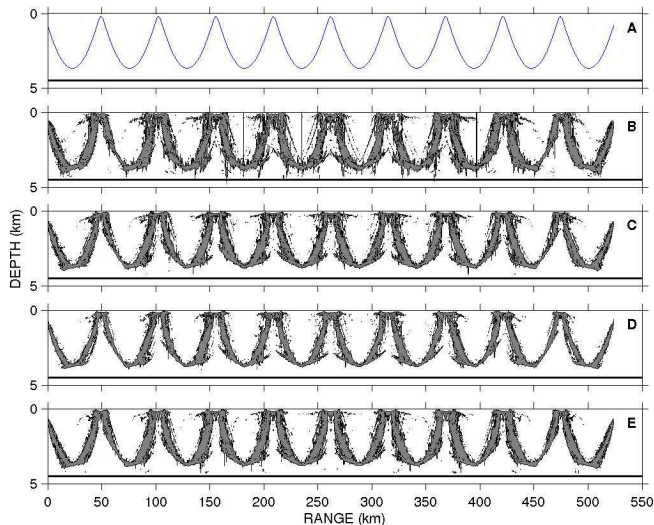


Figure 7: Same as Fig. 6 except for peak 2.

The fractional amplitude method for drawing diffracted regions from Eq. (13) yields diffracted regions that look a little fuzzier and fatter for peak 2 than those using the relative dB method (Figs. 7,8). Results are similar for the other peaks (not shown).

Blowups of the diffracted regions associated with peak 2 near 100 Hz (Fig. 9A) allow better scrutiny of the departures from ray theory. The threshold criteria for the relative dB method is changed to suppress some of the apertures that contribute quieter sounds (Fig. 9B). Further suppression of quieter apertures makes the diffracted regions look discontinuous in space which seems unphysical because there would not be any path joining the source and receiver. Thus the flat regions near the surface that look so unlike rays, and some of the other extensions away from the ray path are significant departures from ray theory.

### A. Importance of accounting for interference on a phase screen in inhomogeneous media

When the effects of interference are not dealt with using Eq. (13), the region of diffraction looks less plausible than otherwise (e.g. peak 2, Figs. 7,10). The difference is due to the fact that some adjacent apertures on phase screens pass large amounts of energy that destructively interfere at the receiver leaving little net energy.

### B. Comparison with Fresnel radius for inhomogeneous medium

The first Fresnel radius for any point A on a ray path between a source and receiver is the distance, perpendicular to the ray at A, to a point B such that the difference of

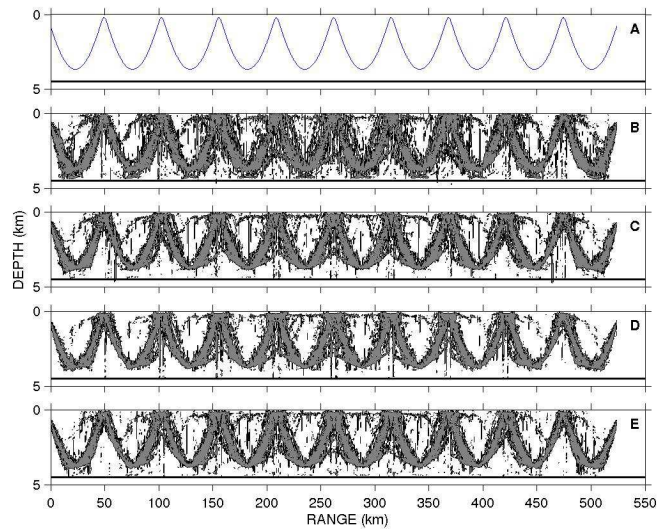


Figure 8: Same as Fig. 7 for peak 2 except this uses the fractional amplitude method with  $f = 0.9$ . These diffracted regions are fuzzier and somewhat wider than obtained using the relative dB method.

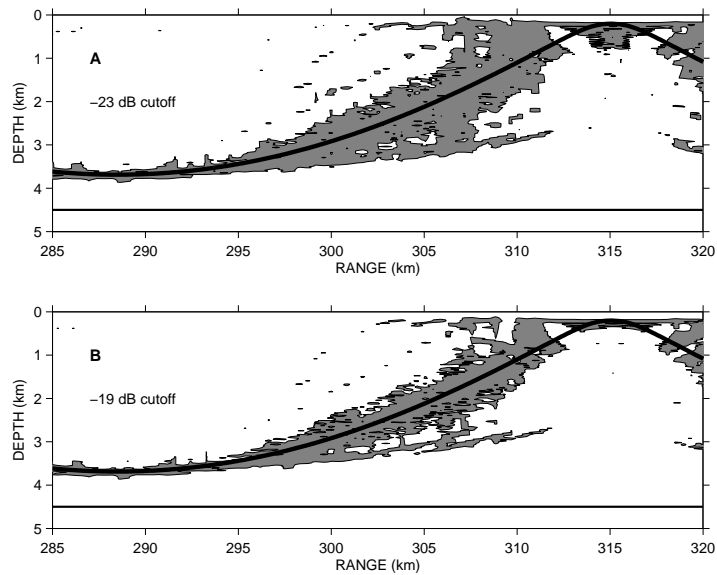


Figure 9: A: Same as Fig. (7C) between ranges of 285 and 320 km with ray path superimposed using a cutoff of  $X_{dB} = -23$  dB. B: Same as A except the cutoff is increased to -19 dB. The center frequency is 100 Hz.

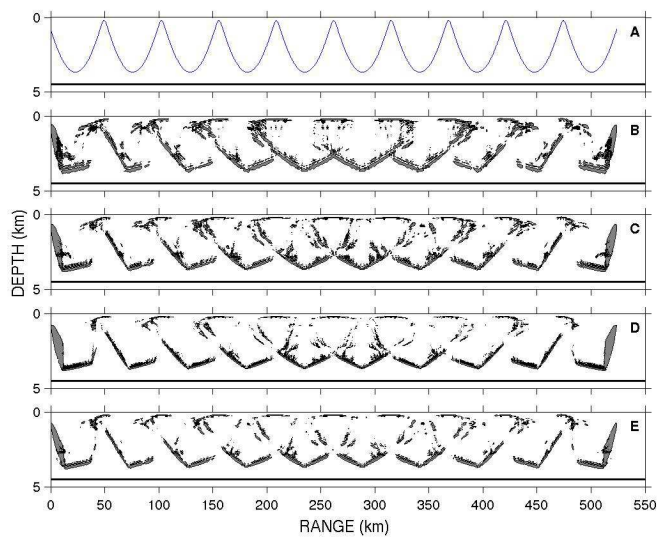


Figure 10: Same as Fig. (7) except the effects of destructive interference between adjacent vertical apertures on phase screens are not corrected using Eq. (13). Instead this estimate of the diffracted regions assumes that adjacent apertures do not interfere with each other, yielding an incorrect picture for where sounds travel. The apertures within 6 dB of the most energetic aperture on each phase screen are shown because when interference is not accounted for, the 6 dB threshold yields the theoretical zone of influence for homogeneous media (not shown).

the signal wavelength is one-half between the ray and the perturbed ray passing through B and back to the receiver. For steeply cycling rays in the deep ocean waveguide such as shown in Figs. (6- 7), first order analysis and more exact numerical evaluations demonstrate the standard result that the Fresnel radius for such rays is zero at its turning points and is approximately the Fresnel radius for an homogeneous medium in-between, i.e. Eq. (5), (see Eq. 7.1.11 in Ref. [4] and Eq. (26) in Ref. [5]). For  $d = 523.845$  km,  $\lambda = 1.5$  km s<sup>-1</sup>/100 Hz = 0.015 km, and  $x = d/2$  (half-way between source and receiver), the Fresnel radius is  $R_f = 1.4$  km. If the Fresnel radius was a good predictor of the region of diffraction, the diffracted region would encompass  $\pm 1.4$  km on either side of the unperturbed ray path near 250 km and go to zero at the turning points of the rays in Figs. (6-7). However, the diffracted region for peaks 1 and 2 extend for a length scale of  $O(0.1)$  km in a direction perpendicular to the unperturbed rays, and a radius of 1.4 km is too large for all the diffracted regions shown. The diffracted region does not go to zero at the turning points.

Replacing the radius of the zone of influence,  $R_I$ , for  $R_f$  does not help this discrepancy because the length scale  $2cT = 2 \times 1.5$  km s<sup>-1</sup>  $\times$  0.05 s = 0.15 km needed by  $R_I$  exceeds  $\lambda = 0.015$  km for  $R_f$  at 100 Hz, making  $R_I$  about 4.5 km. It is unfortunate but not surprising that neither the Fresnel radius nor the zone of influence in Eq. (4) provide the correct scaling for diffracted regions in inhomogeneous media.

## V. VERIFYING ALGORITHMS

It is important to verify the correctness of the algorithms because of the fundamental importance of the results. The strongest evidence for the validity of these results should and must come from other independent investigations. For example, a previous construction of diffracted regions [3] shows that sound lingers longer near the surface than the corresponding ray. This behavior appears in Figs. (6- 7) in a much more pronounced way. There are four other reasons to believe the algorithms are correct.

Firstly, the algorithms for the inhomogeneous case are identical to those for the homogeneous case which agrees with the analytical solution for the zone of influence (Fig. 3). Secondly, the derivation of the integral theorem of Helmholtz and Kirchhoff includes a proof for the reciprocity of the field in a time-independent medium. The  $c_0$  insensitive parabolic approximation in this paper, must also obey reciprocity, and it does [12]. Thirdly, the time series at the receiver should look like the time series computed from the integral theorem of Helmholtz and Kirchhoff after integrating over all depths for any vertical screen between the source and receiver, and they do. Fourthly, results from physical optics [1] look nearly identical to those from the integral theorem of Helmholtz and Kirchhoff for all cases in this paper (not shown) The similarity is due to the fact that sound propagates nearly perpendicular to the vertical phase screens, thus the inclination factor from physical optics should be very near unity as chosen for Eq. (8).

## VI. CONCLUSIONS

A needed last step was added to the integral theorem of Helmholtz and Kirchoff for the purpose of quantifying hierarchical contributions of energy to any specified time window at a receiver from transient emissions from a source. The resulting construction of regions where signals travel appear to be the first of its kind for application in inhomogeneous media. The method introduced here is a fundamental tool in understanding the physics of transient propagation between two points, and is useful for quantifying errors in the theory of rays.

Using the new method, the first Fresnel radius is shown to be an incorrect scale for estimating where transient signals travel between a source and receiver in inhomogeneous media. A scattering theory of sound in the ocean adopts the Fresnel radius for determining which fluctuations affect transient propagation near a ray [4, 5]. A re-interpretation of this theory in light of the findings here should be considered. This paper finds that the regions where signals travel can be complicated, and may defy a simple formula for explaining the physics, such as the Fresnel radius does for single-frequency signals.

A theory that predicts the scattering of sound by internal waves has been shown to not fit observations for an experiment at 75 Hz center frequency and 35 Hz bandwidth over 3250 km in the Pacific [5]. The data are consistent with scattering in the unsaturated or partially unsaturated regime. The theory predicts that scattering should be in the fully saturated regime. The theory would be more consistent with the data if its so-called size parameter,  $\Lambda \sim (R/L)^2$  was several orders of magnitude smaller than its predicted values from 1 to 40 (Fig. 19, Ref. [5]). Here,  $R$  represents the distance perpendicular to an unperturbed ray over which the sound is influenced by fluctuations, and  $L$  is the spatial scale of the fluctuations. Standard theoretical and numerical results from that theory yield  $R = 0$  at the upper turning points of the rays and  $R \sim O(R_f)$  in between which is about 2 km for the 3250 km transmission (Fig. 20, Ref. [5]). For the simulations discussed in **Sec. IVB**, the diffracted regions are an order of magnitude less than the Fresnel radius. If the same was true for the Pacific experiment,  $\Lambda$  would decrease by two orders of magnitude. This would close the gap between theory and observation. The only point of this back-of-the-envelope calculation is to raise the possibility that an accurate calculation of the diffracted region in the Pacific experiment might contribute to a more accurate prediction.

It is important to quantify errors in the ray approximation. At 100 Hz, the wavelength in the sea is 15 m. This *is* small compared with the 1000 m scale of the wave guide (Fig. 4). The results given here suggest this ratio needs to be much smaller to consistently yield ray-like paths. Perhaps the break down of ray theory at low frequencies is due to the boundary conditions at the surface and bottom. It is also possible that the pulse resolution needs to be much smaller than 0.025 s to yield ray-like paths at low frequencies. Of course, there is a practical limit for the pulse resolution at low frequency. The range of validity for Snell's law is apparently not well understood at this time, despite its use for describing sound transmission in the deep sea since 1917 [18]. The advance of computers makes it possible to research this subject in new ways.

## ACKNOWLEDGMENTS

This research was supported by the Office of Naval Research contract N00014-03-C-0155 and by a grant of computer time from the DOD High Performance Computing Modernization Program at the Naval Oceanographic Office. The zray raytrace program was modified from the program written by James Bowlin. I thank Alfred Mann (U. Pennsylvania) and Eugene Terray (Woods Hole), for their constructive and interesting inputs. I thank Joseph Keller (Stanford) for his time in answering my queries about the geometrical theory of diffraction and physical optics.

## References

- [1] Principles of Optics: electromagnetic theory of propagation, interference, and diffraction, M. Born, and E. Wolf, with contributions by A. Bhatia *et al*, Cambridge University Press, Cambridge, (1999).
- [2] A. D. Pearce, Acoustics: an introduction to its physical principles and applications, Acoustical Society of America, 678 pp. (1989).
- [3] J. Bowlin, Generating eigenray tubes from two solutions of the wave equation, J. Acoust. Soc. Am., **89**, 2663-2669 (1991).
- [4] S. M. Flatte, R. Dashen, W. Munk, K. Watson, and F. Zachariasen, Sound transmission through a fluctuating ocean, Cambridge University Press, Cambridge, pp. 299 (1979).
- [5] J. A. Colosi, E. K. Scheer, S. M. Flatte, B. D. Cornuelle, M. A. Dzieciuch, W. H. Munk, P. F. Worcester, B. M. Howe, J. A. Mercer, R. C. Spindel, K. Metzger, T. G. Birdsall, and A. B. Baggeroer, Comparisons of measured and predicted acoustic fluctuations for a 3250-km propagation experiment in the eastern North Pacific Ocean, J. Acoust. Soc. Am., **105**, 3202-3218 (1999).
- [6] A. W. Trorey, A simple theory for seismic diffractions, Geophysics, **35**, 762-784 (1970).
- [7] R. W. Knapp, Fresnel zones in the light of broadband data, Geophysics, **56**, 354-359 (1991).
- [8] M. Bruhl, G. J. O. Vermeer, and M. Kiehn, Fresnel zones for broadband data, Geophysics, **61**, 600-604 (1996).
- [9] B. R. Zavalishin, Diffraction problems of 3D seismic imaging, Geophysical Prospecting, **48**, 631-645 (2000).

- [10] J. Pearce and D. Mittleman, Defining the Fresnel zone for broadband radiation, *Physical Review E*, **66**, 056602 (2002).
- [11] J. B. Keller, Geometrical theory of diffraction, *J. Optical Society of America*, **52**, 116-130 (1962).
- [12] F. Tappert, J. L. Spiesberger, and L. Boden, New full-wave approximation for ocean acoustic travel time predictions, *J. Acoust. Soc. Am.*, **97**, 2771-2782 (1995).
- [13] S. Levitus, Climatological atlas of the world ocean, in NOAA Prof. Pap. 13, U.S. Government Printing Office, Washington, DC, 1982.
- [14] V. A. Del Grosso, New equation for the speed of sound in natural waters with comparisons to other equations, *J. Acoust. Soc. Am.*, **56**, 1084-1091 (1974).
- [15] M.A. Wolfson and J.L. Spiesberger, Full wave simulation of the forward scattering of sound in a structured ocean: A comparison with observations, *J. Acoust. Soc. Am.*, **106**, 1293-1306 (1999).
- [16] J. L. Spiesberger, An updated perspective on basin-scale tomography, *J. Acoust. Soc. Am.*, **109**, 1740-1742 (2001).
- [17] J. B. Bowlin, J. L. Spiesberger, and L. F. Freitag, Ocean acoustical ray-tracing software RAY, Woods Hole Oceanographic Technical Rept., WHOI-93-10, Woods Hole, MA., (1992).
- [18] V. H. Lichte, Über den Einflußhorizontaler Temperaturschichtung des Seewassers auf die Reichweite von Unterwasserschallsignalen, *Physikalische Zeitschrift*, **17**, 385-389 (1919). English translation by A.F. Wittenborn, with a forward by R. J. Urick is available from Woods Hole Oceanographic Institution, Woods Hole, MA. 02543.